Open

Citation: J Med Discov (2025);10(1):jmd25012; DOI:10.24262/jmd.10.1.25012

Research Article

Safety Evaluation of Ginsenoside Rg1-Loaded Conductive Hydrogel for Spinal Cord Injury Treatment in a Rat Model

Jian Lan[1], Ding Lei[1], Lu Lu[2*]

[1] *Youjiang Medical University for Nationalities, Baise, China*

[2] *Youjiang Medical College for Nationalities Affiliated Hospital, Baise, China*

Abstract Spinal cord injury (SCI) induces severe central nervous system damage, leading to debilitating sequelae such as paraplegia, sensory abnormalities, spasticity, neuropathic pain, and cardiovascular dysfunction. These consequences impose a substantial burden on patients and society, highlighting an urgent clinical challenge requiring resolution. Current therapeutic approaches primarily involve surgical intervention and pharmacological treatments, yet both exhibit significant limitations and fail to address secondary damage effects. Neural tissue engineering has proven to be an effective therapeutic strategy, with proper transmission of electrical signals being critical for neuronal survival, growth, and functional expression. Electrically active neural tissue engineering scaffolds can enhance SCI repair through anti-inflammatory effects, immunomodulation, and sustained release of neurotrophic factors. In this study, a polypyrrole-based conductive hydrogel loaded with ginsenoside Rg1 was developed to evaluate its safety and therapeutic efficacy in a rat model of SCI. Results demonstrated that the hydrogel exhibited superior conductivity, excellent hemocompatibility, histocompatibility, and organ compatibility. Furthermore, it significantly promoted tissue repair and functional recovery in SCI rats.

Keywords: Spinal cord injury; Conductive hydrogel; Biocompatibility

How to cite: Jian Lan et al., Safety Evaluation of Ginsenoside Rg1-Loaded Conductive Hydrogel for Spinal Cord Injury Treatment in a Rat Model . J Med Discov (2025); 10(1): jmd25012; DOI:10.24262/jmd.10.1.25012; Received February 02nd, 2025, Revised February 28th, 2025, Accepted March 20th, 2025 , Published March 25th, 2025.

1 Introduction

Spinal cord injury (SCI) refers to structural and functional damage to the intraspinal neural structures—including the spinal cord, nerve roots, and cauda equina—resulting from diverse etiologies. This condition manifests as sensory and motor impairments, diminished reflexes, and bladder/bowel dysfunction below the injury level[1].Neurogenic shock stands as one of the principal causes of mortality following SCI, while the degree of post-injury disability is determined by the severity of the spinal cord lesion[2]. Globally, approximately 574,000 new SCI cases were reported in 2021, with the total prevalent cases reaching an estimated 15.4 million [3].Since 1990, the global incidence rate, prevalence, and years lived with disability (YLD) of SCI have exhibited persistent increases. This upward trend has been accompanied by marked disparities in incidence across nations and regions, with prevalence in high-income areas substantially exceeding the global average—a pattern attributed primarily to elevated rates of traffic accidents, falls (particularly among the elderly), and sports-related injuries [4].SCI induces profound and irreversible impairment to the neurological system. Despite remarkable advancements in biomedical technologies and medical practices, there remains a critical absence of clinically proven regenerative therapies targeting neurological repair, rendering SCI an intractable public health challenge in modern society.

SCI pathophysiologically progresses through two distinct phases: primary injury and secondary injury. Primary injury typically results from mechanical forces such as

*Correspondence: Lu Lu, Youjiang Medical College for Nationalities Affiliated Hospital, Baise, China. E-mail:8869860@qq.com.

acceleration-deceleration trauma during blunt impact, leading to shear-induced axonal tearing and spinal cord fiber disruption. This disrupts the vasculature and blood-spinal cord barrier, culminating in irreversible neuronal damage characterized by immediate cell death, axonal disintegration, and inhibition of axonal regeneration [5].Secondary injury is mechanistically triggered by the primary mechanical insult, initiating a self-perpetuating cascade of biochemical and cellular derangements. These include localized hemorrhage, ischemia, vascular compromise, edema, ionic dysregulation, free radical-mediated oxidative stress, neuroinflammation, lipid peroxidation, free radical accumulation, demyelination, Wallerian degeneration, apoptotic cell death, and disrupted ion homeostasis. These processes collectively establish a hostile microenvironment marked by glial scar formation and cystic cavitation, which chronically impede tissue repair [6]. Over time, such pathological alterations evolve into syringomyelia and gliotic scarring, precipitating irreversible clinical sequelae such as sensory deficits, motor paralysis, and autonomic dysfunction [7, 8]. Critically, both primary and secondary injury mechanisms synergistically exacerbate neurological deficits in SCI patients while creating biochemical and structural barriers to neural repair and regeneration.

Current therapeutic strategies for SCI predominantly encompass surgical intervention, pharmacotherapy, and cell-based therapies. Surgical decompression mitigates mechanical compression of the spinal cord and reperfuses ischemic penumbra, yet fails to directly facilitate axonal repair or regeneration [9]. Pharmacotherapy approaches are constrained by a narrow therapeutic window and systemic adverse effects, with no clinically approved drugs currently available to reliably restore post-SCI motor function [10]. In contrast, neural tissue engineering has emerged as a promising therapeutic paradigm. Engineered neural scaffolds can precisely deliver stem cells to lesion sites, replace and reconstruct damaged neural circuits, provide extracellular matrix support for engrafted cells, and guide topographically organized tissue regeneration [11]. Consequently, scaffold-based regenerative strategies have become a pivotal focus in translational neuroscience research.

Bioelectrical signals critically modulate a spectrum of fundamental biological processes, including angiogenesis, mitogenesis, intercellular signaling, and neuroregeneration [12]. Within the nervous system, the dynamic interplay between neurons and non-neuronal cells is governed by precisely orchestrated electrical activity. The spatiotemporal fidelity of these bioelectrical transmissions is indispensable for neuronal survival, axonal growth, and functional synaptic plasticity [13]. The secondary injury phase post-SCI causes critical neural cell loss, which directly impairs action potential propagation in spinal circuits [14].

Ginsenoside Rg1, a bioactive constituent of Panax ginseng, has been extensively investigated for its anti-inflammatory, antioxidant, and neuroprotective properties in treating neurodegenerative and neuropsychiatric disorders, including dementia and depression [15]. Preconditioning neuronal cells with ginsenoside Rg1 enhances the yield of extracellular vesicles (EVs) that potentiate microglial polarization toward the M2 phenotype, attenuate oxidative stress, reprogram immune responses, and reduce pro-inflammatory cytokine secretion, collectively promoting neurorestoration [16]. Mechanistically, ginsenoside Rg1 upregulates Malat1 expression via miR-124-3p-dependent regulation, activating the

Lamc1/PI3K/AKT signaling axis to modulate astrocytic activation and enhance functional recovery post-spinal cord injury [17].

In this study, we fabricated a polypyrrole-based conductive hydrogel loaded with ginsenoside Rg1 and conducted systematic in vitro and in vivo experiments to evaluate its biocompatibility for spinal cord injury applications.

2 Experimental Section

2.1 Hydrogel Fabrication

In simple terms , GelMA hydrogel (GM): A 10% (w/v)GelMA solution was prepared by dissolving GelMA in0.25% (w/v) Lithium Phenl-2,4-6-trimethylbenzoyl p hosphate (LAP) under light protection, incubated at 5 0°C for 30 min with periodic mixing. The solution wa s transferred to molds and UV-cured (365 nm, 5 mW/ cm^2,20 s).GMP hydrogel: 0.03 g polypyrrole(PPY) wa s added to the GelMA/LAP solution prior to UV curin g (min).GMP-R hydrogel: Ginsenoside Rg1 was blend ed into the GMP precursor (maintaining 10% GelMA) and UV-cured as above.

2.2 Hydrogel Characterization

Fourier-transform infrared spectroscopy (FTIR) was employed to analyze the chemical composition of the GMP-R hydrogel and confirm the successful incorporation of PPY and ginsenoside Rg1. The GMP-R hydrogel was lyophilized for 48 hours prior to testing. For FTIR sample preparation, a mixture of powdered components (GelMA, PPY, and Rg1) with potassium bromide (KBr) at a 1:100 mass ratio was thoroughly ground and pressed into transparent pellets. Spectra were acquired in the mid-infrared range (400-4000 cm^{-1}) with a resolution of 4 cm^{-1}.

2.3 Electrical Conductivity Testing

The electrical conductivity of hydrogels was measured using an RTS-8 four-point probe system. Samples were flattened on the sample stage, and the instrument was calibrated with sample thickness input via testing software. The four probes were rotated to ensure full contact with the sample surface. Three distinct regions per sample were measured. Conductivity was calculated as:

$$\sigma = \frac{1}{Rt}$$

where R is resistance and t is sample thickness. Triplicate measurements were averaged for statistical validity.

2.4 Hemocompatibility Testing

Blood samples (5 mL each) were collected from the abdominal aorta of three adult female SD rats (220±50 g) and evenly distributed into five heparinized tubes. Each tube received 2 mL of normal saline (NS), forming five groups: negative control (NS), positive control (deionized water, DI water), GM , GMP , and GMP-R hydrogel. Equal masses of GM, GMP, and GMP-R hydrogels were immersed in their respective tubes, while NS and DI water were added to negative and positive controls, respectively.Samples were incubated at 37°C for 4 h, followed by centrifugation at 12,000 rpm for 5 min (4°C). Hemolysis was assessed by visually inspecting supernatant coloration and measuring optical density (OD) at 545 nm. The hemolysis rate was calculated using the standard formula:

$$\text{Hemolysis ratio} = \frac{OD(Hydrogel) - OD(NS)}{OD(DI) - OD(NS)}$$

2.5 Animal Model Establishment

Adult female SD rats (220±50 g) were anesthetized intraperitoneally with 2.5% tribromoethanol (1.2 mL/100

g). A 2-mm left spinal cord hemi-section at T10 (lateral to central artery) was created after laminectomy. GMP/GMP-R hydrogels were implanted, followed by layered wound closure. Postoperative care included 3-day penicillin prophylaxis, twice-daily bladder expression, and povidone-iodine disinfection of lower body areas until spontaneous urination resumed.

2.6 Histocompatibility

On day 56 post-modeling, major organs (heart, lungs, liver, kidneys, spleen, and small intestine) were harvested from euthanized rats under anesthesia (2.5% tribromoethanol, 1.2 mL/100 g, i.p.), fixed, dehydrated, and subjected to hematoxylin and eosin (H&E) staining.

2.7 In Vivo Degradation and Biocompatibility

Adult female SD rats (220±50 g) were subcutaneously implanted with uniform-sized GM, GMP, and GMP-R hydrogels in the dorsal region under anesthesia (2.5% tribromoethanol, 1.2 mL/100 g, i.p.). Hydrogels and surrounding tissues were explanted at 7 and 42 days post-implantation for H&E staining. Inflammatory layer thickness at the implantation site was quantified using Image J software.

2.8 Behavioral Assessment

Motor functional recovery was evaluated weekly for 8 consecutive weeks using the Basso-Beattie-Bresnahan (BBB) locomotor rating scale, followed by footprint analysis at week 8. For BBB scoring, rats were allowed to ambulate freely for 5 min in an open field. Gait quantification was performed by coating forelimbs and hindlimbs with blue and red ink respectively, followed by linear walking trials on a custom-designed runway to record and quantify gait patterns.

2.9 Histological Analysis

At 8 weeks post-surgery, rats underwent transcardial perfusion with physiological saline followed by 4% paraformaldehyde. The spinal cord at the lesion site was dissected, fixed, dehydrated, and subjected to H&E staining.

2.10 Statistical Analysis

Data were analyzed using SPSS 24.0. Continuous variables are expressed as mean ± standard deviation (SD). Intergroup comparisons were performed with Student's t-test for two groups. For multi-group comparisons, normality was verified using Shapiro-Wilk tests, followed by one-way ANOVA with F-test for homogeneity of variance (equal variances assumed) or Kruskal-Wallis test for heterogeneity (equal variances not assumed). Statistical significance was defined as $p < 0.05$.

3 Results

3.1 Synthesis and Characterization of GMP-R Hydrogels

The gelatin-based conductive hydrogel fabrication process is illustrated in Fig. 1A. All pre-photocrosslinked formulations remained liquid, while UV irradiation induced successful solidification. FTIR analysis (Fig.1B) revealed characteristic bands of ginsenoside Rg1: C-H stretching vibrations (2988 cm^{-1}), C-H wagging coupled with hydroxyl deformation vibrations (1448 cm^{-1}), and a broad O-H stretching vibration (3200-3500 cm^{-1}). Gelatin exhibited signature absorptions at 1650 cm^{-1} (amide I, C=O stretching) and 1440 cm^{-1} (amide III, N-H/C-H planar vibrations). PPY powder displayed diagnostic peaks at 1544 cm^{-1} (pyrrole ring vibration) and 1034 cm^{-1} (C-H in-plane deformation). The GMP-R hydrogel spectrum exhibited characteristic bands at 1034.5 cm^{-1}, 1455.8 cm^{-1}, 1647.5 cm^{-1}, and 3200-3500 cm^{-1}, confirming successful integration of PPY and ginsenoside Rg1 into the

gelatin-methacrylate matrix.

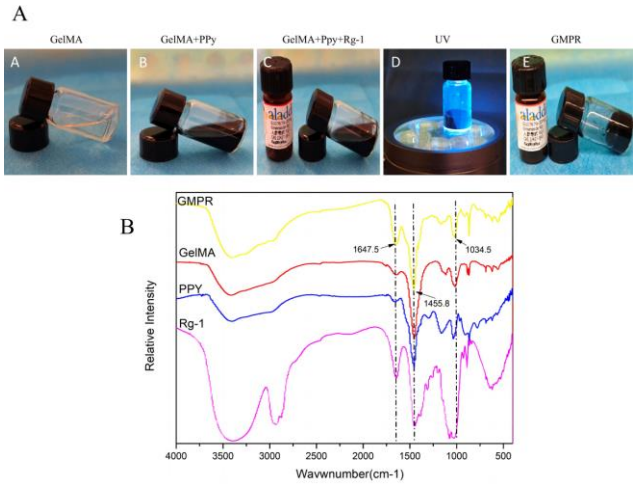

Figure 1. Preparation and characterization of the hydrogel.(A) Schematic illustration of hydrogel fabrication and photocuring process; (B) FTIR spectroscopy analysis of GMP-R hydrogel.

3.2 Electrical Properties of Conductive Hydrogels

As shown in Fig.2A, conventional hydrogels exhibited no electrical conductivity, and GM hydrogels failed to illuminate LED bulbs in closed circuits. In contrast, polypyrrole-incorporated GMP-R hydrogels successfully powered LED bulbs, confirming electromechanical functionality through conductive polymer integration. Four-point probe measurements (Fig.2B) revealed GM hydrogels exceeded resistivity detection limits (no quantifiable conductivity), whereas polypyrrole-modified hydrogels (GMP/GMP-R groups) demonstrated significant conductivity enhancement. Statistical analysis confirmed a marked difference ($p < 0.01$) in conductivity between GM and polypyrrole-containing hydrogels.

3.3 Biocompatibility of Conductive Hydrogels

Hemocompatibility, a critical quantitative indicator for biomaterials, requires medical materials to exhibit hemolysis rates below 5% per ISO 10993 series standards. In hemolytic assays, deionized water and physiological saline served as positive and negative controls, respectively, for evaluating GM, GMP, and GMP-R hydrogels. Macroscopic observations (Fig.3A) revealed complete erythrocyte lysis in positive controls (bright red coloration), whereas negative controls and hydrogel-treated groups maintained clear pale yellow supernatants, indicating minimal hemolysis. Quantitative analysis (Fig.3B) via supernatant absorbance (OD) demonstrated hemolysis rates of 2.69% (GM), 1.88% (GMP), and 0.34% (GMP-R), all complying with ISO 10993 requirements (<5% threshold).Eight weeks post-implantation in SCI rats, H&E staining of major organs(Fig.3C) revealed:Heart: Tightly aligned cardiomyocyte bundles with distinct striations, absent inflammatory infiltration;Lungs: Intact thin-walled alveoli without structural collapse or inflammatory exudates;Liver: Preserved hepatic lobule architecture with no fibrosis or necrotic foci around central veins;Kidneys: Normal glomerular morphology and proximal tubules, devoid of protein casts or metabolic overload indicators; Spleen: Well-defined white pulp germinal centers and physiological red pulp macrophage-erythrocyte ratios;Intestine: Regular crypt-villus architecture without inflammatory or necrotic alterations. These findings demonstrate excellent biocompatibility of GMP-R hydrogels with vital organs, indicating no detectable systemic toxicity.Subcutaneous implantation of three hydrogel groups in rats revealed time-dependent degradation profiles (Fig.3D). At day 7 post-implantation, all hydrogels exhibited increased width and thickness compared to pre-implantation dimensions. By day 42, macroscopic observation demonstrated significant hydrogel thinning, indicative of progressive degradation. H&E staining of peri-implant tissues showed inflammatory cell infiltration at hydrogel-tissue interfaces across groups. Quantitative analysis (Fig.3E,F) measured inflammatory

layer thicknesses of 0.088±0.019 mm (GMP-R, day 7) and 0.013±0.005 mm (GMP-R, day 42). All hydrogel groups displayed significantly thicker inflammatory layers than sham controls at both timepoints ($P < 0.01$), with decreasing thickness trends over time. Notably, GMP-R hydrogels maintained inflammatory layer dimensions closest to native tissue levels.

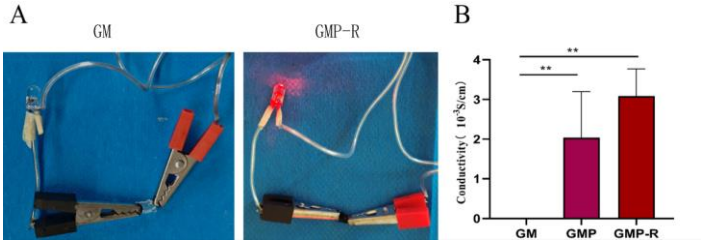

Figure 2. Electrical properties of the hydrogel. (A) Hydrogel functioning as a conductive bridge in a circuit, with the GMP-R hydrogel group successfully illuminating an LED indicator;(B) Electrical conductivity comparison of GM, GMP, and GMP-R hydrogels (**P < 0.01).Electrical conductivity comparison of GM, GMP, and GMP-R hydrogels (**P < 0.01).

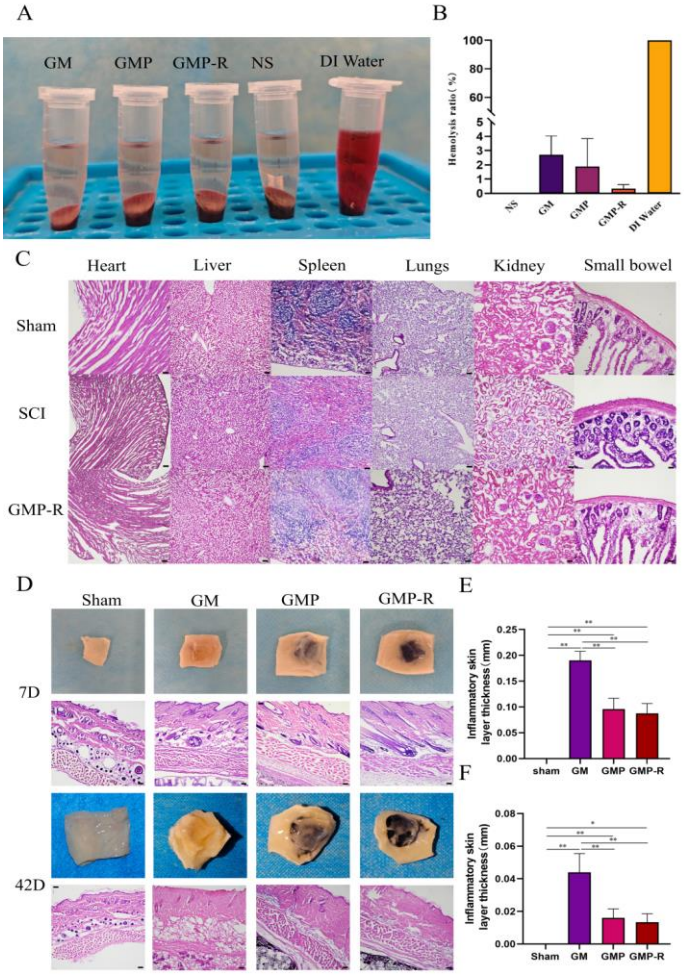

Figure 3. Biocompatibility of the hydrogel. (A)Macroscopic hemolysis observations of different hydrogel groups;(B) Hemolysis ratios of different hydrogel groups;(C) Hematoxylin and eosin (HE) staining of major organs in rats 8 weeks post-implantation;(D) Macroscopic views and HE staining of subcutaneously implanted hydrogels at 7 and 42 days post-implantation;(E) Inflammatory layer thickness in skin tissue at day 7 post-subcutaneous implantation;(F) Inflammatory layer thickness in skin tissue at day 42 post-subcutaneous implantation (*$P < 0.05$, **$P < 0.01$).

3.4 Functional Recovery and Tissue Repair Enhancement by Conductive Hydrogels

Serial Basso-Beattie-Bresnahan (BBB) locomotor ratings over 8 postoperative weeks demonstrated differential recovery patterns (Fig.4A). Sham-operated rats maintained normal locomotor function throughout, whereas other groups showed progressive hindlimb functional improvement. The SCI group exhibited no functional recovery at week 1, developing extensive three-joint movement by week 8 without weight-bearing locomotion. In contrast, GMP and GMP-R groups displayed accelerated recovery, achieving sustained forelimb-hindlimb coordinated gait by week 8. Notably, GMP-R hydrogels enabled forelimb plantar stepping with active paw alignment parallel to the torso during weight-bearing transitions.Gait quantification at 8 weeks postoperatively (Fig. 4B) demonstrated distinct recovery patterns. Footprint analysis revealed blurred hindpaw imprints with persistent dragging marks in SCI rats. Both GMP and GMP-R groups exhibited well-defined plantar impressions without dragging artifacts. While GMP-implanted rats displayed weight-bearing strides with compact hindlimb step cycles, the GMP-R group showed longer, uniform stride lengths and synchronized forelimb-hindlimb gait coordination. These findings confirm that GMP-R hydrogels significantly enhanced coordinated locomotor recovery in

SCI rats.

H&E staining of spinal cord tissues harvested at 8 weeks post-surgery (Fig. 4C) revealed distinct pathological features. Compared to the sham group, all experimental groups exhibited variably sized cavities at lesion sites. Dark conductive particles were observed within the injured areas of GMP and GMP-R groups. These groups displayed clearer tissue organization and sharper gray-white matter demarcation compared to the SCI group. The GMP-R group demonstrated better-preserved overall tissue architecture with reduced inflammatory cell infiltration around the lesion. Quantitative analysis confirmed that the GMP-R group had significantly smaller cavity areas than other groups ($P < 0.01$), closest to those in the sham group.

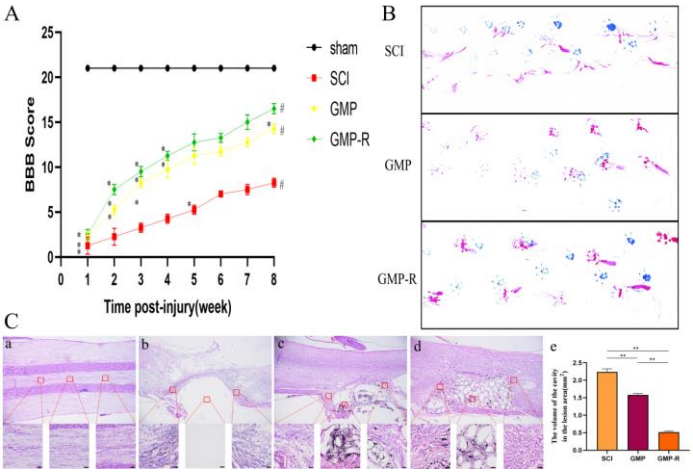

Figure 4. Conductive hydrogel improves tissue repair and functional recovery.(A) Basso, Beattie, Bresnahan (BBB) locomotor rating scores over 8 consecutive weeks post-implantation;(B) Footprint analysis at 8 weeks post-implantation;(C) Hematoxylin and eosin (HE) staining of spinal cord tissues: (a) Sham group; (b) SCI group; (c) GMP group; (d) GMP-R group; (e) Quantification of spinal cavity areas across groups (**$P < 0.01$).

4 Discussion

Spinal cord injury disrupts functional connectivity between supraspinal centers and spinal circuits, resulting in severe motor, sensory, and autonomic dysfunction accompanied by diverse complications that critically impair patients' quality of life and longevity while imposing substantial psychological and socioeconomic burdens [18]. The pathophysiology of SCI encompasses multifaceted processes including ischemia-hypoxia, oxidative stress, neuroinflammation, reactive gliosis, and fibrotic scar formation [19]. Notably, spinal cord-mediated systemic immune regulation and visceral control mechanisms predispose chronic SCI patients to multi-organ inflammatory responses and physiological dysregulation, escalating risks of opportunistic infections and metabolic disorders that accelerate mortality [20]. Current therapeutic paradigms predominantly rely on surgical decompression and methylprednisolone pulse therapy, modalities constrained by limited efficacy. This therapeutic impasse underscores the urgent need for innovative regenerative strategies.

The limitations of conventional SCI therapies and post-injury rehabilitation have driven rapid development of innovative strategies, including neural tissue engineering [21],stem cell transplantation [22], mitochondrial augmentation [23], immunomodulation [24], organoid reconstruction [25], and brain-computer interfaces [26], which have emerged as promising therapeutic modalities with encouraging preclinical outcomes. Notably, advances in neural tissue engineering now offer unprecedented repair strategies for SCI, with hydrogel-based scaffolds representing a particularly active research frontier due to their biomimetic extracellular matrix properties.An ideal hydrogel scaffold must meet the following criteria: (1) biocompatibility; (2) appropriate mechanical strength; (3) controllable degradation rate; (4) optimized pore size, porosity, and 3D architecture; (5) high surface area-to-volume ratio [27].To address microenvironmental impairment post-SCI that limits stem cell transplantation

efficacy, Song et al.[28] developed a bioactive supramolecular nanofiber hydrogel functionalized with insulin-like growth factor-1 (IGF-1). The engineered hydrogel activates IGF-1 downstream signaling pathways to inhibit neural stem cell (NSC) apoptosis, while enhancing neurite outgrowth and remyelination through targeted enrichment of axon regeneration- and remyelination-associated miRNAs combined with extracellular vesicle (EV) uptake, thereby directing NSC differentiation toward synaptic growth and myelin regeneration .WAN et al.[29] engineered an injectable hydrogel by pre-loading azithromycin nanoparticle-modified bone marrow mesenchymal stem cells (BMSCs), which demonstrated localized anti-inflammatory effects via M2 macrophage polarization upregulation, exhibiting neuroprotective efficacy in both in vitro and in vivo models . gelatin methacryloyl (GelMA) hydrogel through free radical-mediated modification of methacrylate groups on gelatin molecules, combining photoinitiator-enabled photocrosslinking. This system preserves gelatin's intrinsic biocompatibility, controllable degradability, and low immunogenicity, while achieving tunable mechanical strength through concentration adjustments, establishing it as a premier candidate for neural tissue engineering applications [30].

This study developed a bioengineered scaffold using GelMA hydrogel as the matrix, doped with PPY to confer electrical conductivity, and functionalized with ginsenoside Rg1 to fabricate the GMP-R composite hydrogel. Systematic biosafety assessments were conducted to validate its applicability for SCI repair. FTIR verified the successful synthesis of GMP-R hydrogel.During the pathophysiological progression of SCI, early-phase microglial activation exerts neuroprotective effects by containing lesion expansion. However, within 2-3 days post-injury, activated microglia induce macrophage infiltration into the injury site, triggering secondary inflammation. These infiltrating macrophages persist beyond 42 days in the lesion microenvironment, critically mediating chronic inflammatory cascades [31].In our hydrogel degradation assay, volumetric expansion was observed at 7 days post-implantation, attributable to swelling behavior, with the slow initial degradation rate providing structural bridging support in acute SCI microenvironments. By 42 days, the hydrogel thickness showed significant reduction compared to the 7-day timepoint while maintaining partial structural integrity, thereby counteracting macrophage-mediated chronic inflammation while meeting long-term neural repair requirements.Quantitative analysis revealed progressive thinning of the peri-implant inflammatory layer in subcutaneous models, with the GMP-R hydrogel group demonstrating minimal inflammatory encapsulation (0.013±0.005 mm) at 42 days, closest to normal skin tissue architecture. Hemocompatibility assessments confirmed a 0.34% hemolysis rate for GMP-R hydrogel, compliant with ISO standards for medical biomaterials (ISO 10993-4:2017). Systemic biosafety evaluation via H&E staining showed preserved histoarchitecture of major organs without pathological inflammation or tissue damage, indistinguishable from negative controls, confirming no systemic toxicity.These data collectively demonstrate the scaffold's favorable biocompatibility and degradation kinetics, fulfilling critical safety criteria for neural regenerative applications.

Electrical stimulation modulates neuronal intracellular Ca^{2+} dynamics via voltage-gated calcium channels, upregulating brain-derived neurotrophic factor(BDNF) and cyclic

adenosine monophosphate(AMP) to enhance regeneration-associated gene expression (Tα1-tubulin, growth-associated protein 43) [32]. This cascade activates c-AMP response element-binding protein (CREB) while suppressing RhoA signaling in the p75 neurotrophin receptor (p75NTR)-Nogo pathway, thereby augmenting cytoskeletal reorganization and neurite extension. Concurrently, elevated BDNF and growth factors orchestrate Schwann cell-mediated remyelination in damaged neural tissues [33].Furthermore, electrical stimulation activates autophagy through mTOR pathway inhibition, promoting neural stem cell differentiation, neuronal maturation, and axonal regeneration [34]. Post-SCI residual neural circuits exhibit spontaneous neuroplastic reorganization, where targeted interventions like electrical stimulation synergize with cell transplantation strategies to amplify functional recovery [35].Recent studies have engineered exosome-laden conductive hydrogels incorporating bone marrow stem cell-derived exosomes, which modulate glial cell polarization and enhance neural stem cell recruitment/differentiation via coordinated regulation of NF-κB and PTEN/PI3K/AKT/mTOR pathways, ultimately promoting axonal regeneration. These findings underscore the critical role of bioelectrical signaling in spinal cord injury repair [36]. PPY, a conjugated polymer widely utilized in tissue engineering, demonstrates exceptional electrical activity and biocompatibility alongside facile synthesis [37].The native spinal cord demonstrates an electrical conductivity of approximately 4.2×10-4S/cm [38].The incorporation of PPY endowed the hydrogel with electroconductive properties. Electrochemical characterization revealed that GMP-R hydrogels exhibited low impedance (4.72±0.84×10-3S/cm conductivity) and demonstrated superior signal transmission within critical threshold ranges. This optimized electrophysiological profile facilitates enhanced intercellular electrical communication and promotes neural circuit remodeling.

To address limitations of conventional SCI therapies, next-generation neural scaffolds have been engineered for in vivo applications. Chen et al.[39] developed an injectable hydrogel with temporally programmed drug release responsive to reactive oxygen species and matrix metalloproteinases , which significantly enhanced SCI recovery through coordinated anti-inflammatory effects, angiogenesis, and neural stem cell differentiation. Liu et al.[40] created an injectable micro-environment-modulating composite hydrogel （AhCeO（2）-Gel） that promotes NSC differentiation via cAMP/PKA pathway activation while inducing microglial M2 polarization, synergistically enhancing axonal regrowth and remyelination.This study investigated spinal cord repair using hydrogels implanted in a hemisection SCI model. Behavioral assessment via BBB scores demonstrated progressive improvement across all groups from weeks 1 to 8, with the GMP-R group achieving functional recovery closest to sham-operated controls and showing statistically significant differences compared to other experimental groups. Gait analysis revealed well-defined paw prints and balanced stride patterns in GMP-R-treated rats, contrasting sharply with the hindlimb dragging observed in untreated SCI animals. Histological examination identified cavity formation in all groups, while conductive hydrogel groups exhibited residual black electroactive particles. Notably, GMP-R hydrogels promoted substantial neo-tissue formation at injury sites with markedly reduced inflammatory infiltration compared to controls, corroborating their favorable degradability,

biocompatibility, and dual efficacy in tissue regeneration and functional restoration.

This investigation acknowledges limitations in comprehensively assessing the hydrogel's mechanical properties, cytocompatibility, and safety implications under exogenous electrical stimulation.

5 Conclusion

SCI remains a formidable clinical challenge due to its complex pathophysiology and devastating consequences. To overcome limitations of conventional therapies, neural tissue engineering strategies integrating microenvironmental restoration and electrophysiological reconstruction have demonstrated significant therapeutic potential. Building upon this framework, we developed a ginsenoside Rg1-incorporated conductive hydrogel that fulfills essential prerequisites for clinical translation, exhibiting optimal structural characteristics and superior tissue compatibility. The synergistic integration of neuroregenerative phytochemicals with electroactive substrates conferred remarkable efficacy in spinal tissue reconstruction and functional recovery post-SCI. This biomimetic approach establishes a novel paradigm for future mechanistic investigations in neuroregenerative medicine.

Conflict of Interests

The authors declare no conflict of interest regarding the publication of this paper.

Conflict of funding statement

None.

References

1. AHUJA C S, WILSON J R, NORI S, et al. Traumatic spinal cord injury[J]. Nat Rev Dis Primers, 2017,3: 17018.
2. QUADRI S A, FAROOQUI M, IKRAM A, et al. Recent update on basic mechanisms of spinal cord injury[J]. Neurosurg Rev, 2020,43(2): 425-441.
3. LU Y, SHANG Z, ZHANG W, et al. Global, regional, and national burden of spinal cord injury from 1990 to 2021 and projections for 2050: A systematic analysis for the Global Burden of Disease 2021 study[J]. Ageing Res Rev, 2025,103: 102598.
4. SAFDARIAN M, TRINKA E, RAHIMI-MOVAGHAR V, et al. Global, regional, and national burden of spinal cord injury, 1990–2019: a systematic analysis for the Global Burden of Disease Study 2019[J]. The Lancet Neurology, 2023,22(11): 1026-1047.
5. LIU X, ZHANG Y, WANG Y, et al. Inflammatory Response to Spinal Cord Injury and Its Treatment[J]. World Neurosurg, 2021,155: 19-31.
6. ANJUM A, YAZID M D, FAUZI DAUD M, et al. Spinal Cord Injury: Pathophysiology, Multimolecular Interactions, and Underlying Recovery Mechanisms[J]. Int J Mol Sci, 2020,21(20).
7. GORITZ C, DIAS D O, TOMILIN N, et al. A pericyte origin of spinal cord scar tissue[J]. Science, 2011,333(6039): 238-242.
8. FAN H, ZHANG K, SHAN L, et al. Reactive astrocytes undergo M1 microglia/macrohpages-induced necroptosis in spinal cord injury[J]. Mol Neurodegener, 2016,11: 14.
9. KARSY M, HAWRYLUK G. Modern Medical Management of Spinal Cord Injury[J]. Curr Neurol Neurosci Rep, 2019,19(9): 65.
10. HASHEMIZADEH S, HOSSEINDOOST S, OMIDI A, et al. Novel therapeutic approach to slow down the inflammatory cascade in acute/subacute spinal cord injury: Early immune therapy with lipopolysaccharide enhanced neuroprotective effect of combinational therapy of granulocyte colony-stimulating factor and bone-marrow mesenchymal stem cell in spinal cord injury[J]. Front Cell Neurosci, 2022,16: 993019.
11. KNOWLTON S, ANAND S, SHAH T, et al. Bioprinting for Neural Tissue Engineering[J]. Trends Neurosci, 2018,41(1): 31-46.
12. HOSOYAMA K, AHUMADA M, GOEL K, et al.

Electroconductive materials as biomimetic platforms for tissue regeneration[J]. Biotechnol Adv, 2019,37(3): 444-458.

13. LUO Y, FAN L, LIU C, et al. An injectable, self-healing, electroconductive extracellular matrix-based hydrogel for enhancing tissue repair after traumatic spinal cord injury[J]. Bioact Mater, 2022,7: 98-111.
14. CANGELLARIS O V, GILLETTE M U. Biomaterials for Enhancing Neuronal Repair[J]. Frontiers in Materials, 2018,5.
15. YANG S, WANG J, CHENG P, et al. Ginsenoside Rg1 in neurological diseases: From bench to bedside[J]. Acta Pharmacol Sin, 2023,44(5): 913-930.
16. [16] RONG Y, WANG J, HU T, et al. Ginsenoside Rg1 Regulates Immune Microenvironment and Neurological Recovery After Spinal Cord Injury Through MYCBP2 Delivery via Neuronal Cell-Derived Extracellular Vesicles[J]. Adv Sci (Weinh), 2024,11(31): e2402114.
17. ZHU Y, ZOU W, SUN B, et al. Ginsenoside Rg1 Regulates the Activation of Astrocytes Through lncRNA-Malat1/miR-124-3p/Lamc1 Axis Driving PI3K/AKT Signaling Pathway, Promoting the Repair of Spinal Cord Injury[J]. CNS Neurosci Ther, 2024,30(11): e70103.
18. TIAN T, ZHANG S, YANG M. Recent progress and challenges in the treatment of spinal cord injury[J]. Protein Cell, 2023,14(9): 635-652.
19. SRIVASTAVA E, SINGH A, KUMAR A. Spinal cord regeneration: A brief overview of the present scenario and a sneak peek into the future[J]. Biotechnol J, 2021,16(9): e2100167.
20. DISABATO D J, MARION C M, MIFFLIN K A, et al. System failure: Systemic inflammation following spinal cord injury[J]. Eur J Immunol, 2024,54(1): e2250274.
21. KWOKDINATA C, CHEW S Y. Additive manufacturing in spatial patterning for spinal cord injury treatment[J]. Adv Drug Deliv Rev, 2025,218: 115523.
22. HOSSEINI S M, BORYS B, KARIMI-ABDOLREZAEE S. Neural stem cell therapies for spinal cord injury repair: an update on recent preclinical and clinical advances[J]. Brain, 2024,147(3): 766-793.
23. JIANG X, WANG W, TANG J, et al. Ligand-Screened Cerium-Based MOF Microcapsules Promote Nerve Regeneration via Mitochondrial Energy Supply[J]. Adv Sci (Weinh), 2024,11(6): e2306780.
24. YANG C, CAI Y X, WANG Z F, et al. Tertiary lymphoid structures in the central nervous system[J]. Trends Mol Med, 2024.
25. XU J, FANG S, DENG S, et al. Generation of neural organoids for spinal-cord regeneration via the direct reprogramming of human astrocytes[J]. Nat Biomed Eng, 2023,7(3): 253-269.
26. LORACH H, GALVEZ A, SPAGNOLO V, et al. Walking naturally after spinal cord injury using a brain-spine interface[J]. Nature, 2023,618(7963): 126-133.
27. CAI M, CHEN L, WANG T, et al. Hydrogel scaffolds in the treatment of spinal cord injury: a review[J]. Front Neurosci, 2023,17: 1211066.
28. SONG P, HAN T, WU Z, et al. Transplantation of Neural Stem Cells Loaded in an IGF-1 Bioactive Supramolecular Nanofiber Hydrogel for the Effective Treatment of Spinal Cord Injury[J]. Adv Sci (Weinh), 2024,11(17): e2306577.
29. WAN Y, LIN Y, TAN X, et al. Injectable Hydrogel To Deliver Bone Mesenchymal Stem Cells Preloaded with Azithromycin To Promote Spinal Cord Repair[J]. ACS Nano, 2024,18(12): 8934-8951.
30. [30] PUCKERT C, TOMASKOVIC-CROOK E, GAMBHIR S, et al. Electro-mechano responsive properties of gelatin methacrylate (GelMA) hydrogel on conducting polymer electrodes quantified using atomic force microscopy[J]. Soft Matter, 2017,13(27): 4761-4772.
31. BHATT M, SHARMA M, DAS B. The Role of Inflammatory Cascade and Reactive Astrogliosis in Glial Scar Formation Post-spinal Cord Injury[J]. Cell Mol Neurobiol, 2024,44(1): 78.
32. PELTIER J, O'NEILL A, SCHAFFER D V. PI3K/Akt and CREB regulate adult neural hippocampal progenitor proliferation and differentiation[J]. Dev Neurobiol, 2007,67(10): 1348-1361.
33. ZHU R, SUN Z, LI C, et al. Electrical stimulation affects neural stem cell fate and function in vitro[J]. Exp Neurol, 2019,319: 112963.
34. HE L, SUN Z, LI J, et al. Electrical stimulation at nanoscale topography boosts neural stem cell neurogenesis through the enhancement of autophagy signaling[J]. Biomaterials, 2021,268: 120585.
35. ANDERSON M A, SQUAIR J W, GAUTIER M, et al. Natural and targeted circuit reorganization after spinal cord injury[J]. Nat Neurosci, 2022,25(12): 1584-1596.
36. FAN L, LIU C, CHEN X, et al. Exosomes-Loaded Electroconductive Hydrogel Synergistically Promotes Tissue Repair after Spinal Cord Injury via Immunoregulation and Enhancement of Myelinated Axon Growth[J]. Adv Sci (Weinh), 2022,9(13): e2105586.
37. ATEH D D, NAVSARIA H A, VADGAMA P.

Polypyrrole-based conducting polymers and interactions with biological tissues[J]. J R Soc Interface, 2006,3(11): 741-752.

38. FAN C, YANG W, ZHANG L, et al. Restoration of spinal cord biophysical microenvironment for enhancing tissue repair by injury-responsive smart hydrogel[J]. Biomaterials, 2022,288: 121689.
39. CHEN H, WANG W, YANG Y, et al. A sequential stimuli-responsive hydrogel promotes structural and functional recovery of severe spinal cord injury[J]. Biomaterials, 2025,316: 122995.
40. LIU D, NIU R, WANG S, et al. Nitric Oxide-Releasing Mesoporous Hollow Cerium Oxide Nanozyme-Based Hydrogel Synergizes with Neural Stem Cell for Spinal Cord Injury Repair[J]. ACS Nano, 2025,19(2): 2591-2614.